Acta Cryst E CRYSTALLOGRAPHIC COMMUNICATIONS
ISSN 2056-9890

Synthesis, crystal structure and Hirshfeld surface analysis of the orthorhombic polymorph of 4-bromo-*N*-(4-bromobenzylidene)aniline

A. Subashini,[a,b]* K. Ramamurthi,[b] R. Ramesh Babu,[b] Reji Philip[c] and Helen Stoeckli-Evans[d]*

[a]PG and Research Department of Physics, Arts and Science College, Tiruchirappalli - 620 005, India, [b]Crystal Growth and Thin Film Laboratory, Department of Physics, Bharathidasan University, Tiruchirappalli - 620 024, India, [c]Ultrafast and Nonlinear Optics Laboratory, Raman Research Institute, C. V. Raman Avenue, Sadashivanagar, Bangalore 560 080, India, and [d]Institute of Physics, University of Neuchâtel, rue Emile-Argand 11, 2000 Neuchâtel, Switzerland. *Correspondence e-mail: viji.suba@gmail.com, helen.stoeckli-evans@unine.ch

Received 9 January 2023
Accepted 5 February 2023

Edited by W. T. A. Harrison, University of Aberdeen, United Kingdom

Keywords: crystal structure; *N*-benzylideneaniline; polymorphism; Hirshfeld surface; fluorescence; two-photon absorption.

CCDC reference: 1583365

Supporting information: this article has supporting information at journals.iucr.org/e

The crystal structure of the title compound, $C_{13}H_9Br_2N$ [systematic name: (*E*)-*N*,1-bis(4-bromophenyl)methanimine], is a second polymorph (Form II) crystallizing in the orthorhombic space group *Pccn*. The first polymorph (Form I) crystallizes in the monoclinic space group $P2_1/c$ [Bernstein & Izak (1975). *J. Cryst. Mol. Struct.* **5**, 257–266; Marin *et al.* (2013). *J. Mol. Struct.* **1049**, 377–385]. The molecule is disordered about an inversion center situated in the middle of the C=N bond, similar to the situation in the monoclinic polymorph: the C=N bond length is 1.243 (7) Å. In the crystal, molecules stack along the *b*-axis direction and are linked by C—H···π interactions. The interatomic contacts in the crystal for both polymorphs were studied by Hirshfeld surface analysis and have notable differences. The solid-state fluorescence spectrum of Form II shows an emission peak at *ca* 469 nm. The two-photon absorption coefficient measured from the open aperture *Z*-scan technique is 1.3 × 10^{-11} m W^{-1}, hence, Form II shows optical limiting behaviour.

1. Chemical context

Many compounds possess the ability to form polymorphs (Rolf, 2006; Caira, 2017) and polymorphism and disorder are well established in *N*-benzylideneaniline compounds. Homo-disubstituted benzylideneaniline compounds such as *N*-(4-chlorobenzylidene)-4-chloroaniline (Bernstein & Schmidt, 1972; Bernstein & Izak, 1976) and *N*-(4-methylbenzylidene)-4-methylaniline (Bar & Bernstein, 1977, 1982; Bernstein & Izak,1976) exist in dimorphic and trimorphic forms, respectively. Bar & Bernstein (1983) reported a detailed description of three types of disorder in *N*-benzylideneanilines, *viz*., positional, orientational and substitutional. These various types of disorder have been discussed in relation to hetero-disubstituted 4-*X*-*N*-(4′-nitrobenzlidene)anilines (where *X* = H, F, Cl, Br, CH_3, CH_3O, OH) by Leela *et al.* (2020 and references therein).

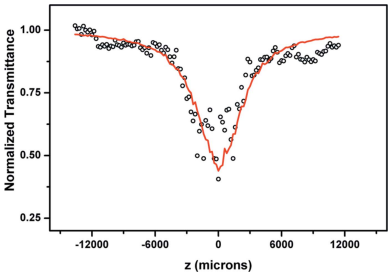

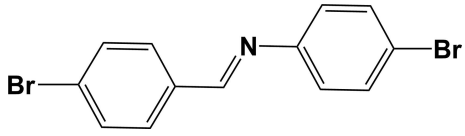

The crystal structure of the monoclinic polymorph of the title compound, *N*-4-bromobenzylidene)-4-bromoaniline, $C_{13}H_9Br_2N$ (Form I) has been reported by Bernstein & Izak (1975) and later by Marin *et al.* (2013). Bernstein & Hagler

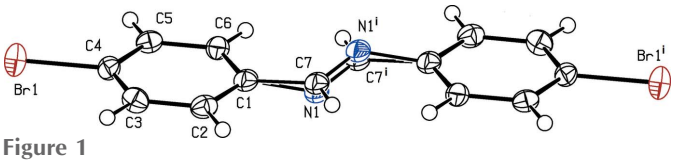

Figure 1
A view of the molecular structure of Form II of the title compound, with atom labelling. Displacement ellipsoids are drawn at the 50% probability level. Symmetry code: (i) $-x, -y, -z$.

(1979) stated that they did not observe polymorphism for this compound. However, Marin *et al.* (2013) reported that a second polymorph could appear during thermal treatment.

In the present study the homo-disubstituted title compound was synthesized using the procedure described by Bernstein & Izak (1975). Single crystals were grown by slow evaporation of a solution in either ethanol or a mixture of methanol/chloroform (1:1). Crystals from both essays proved to be those of the orthorhombic polymorph – Form II.

2. Structural commentary

The title compound crystallizes in the orthorhombic space group *Pccn* (Form II). It exhibits disorder about a crystallographic inversion center situated on the middle of the C7═N1 bond, as illustrated in Fig. 1. This arrangement is similar to that observed for the monoclinic polymorph (Bernstein & Izak, 1975; Marin *et al.*, 2013) and for the orthorhombic and monoclinic polymorphs of the chloro-disubstituted *N*-benzylideneaniline (Bernstein & Izak, 1976; Bernstein & Schmidt, 1972).

Atoms C7, H7 and N1 were refined with occupancies of 0.5 each. The C═N bond length is 1.243 (7) Å, and the benzene rings are co-planar by symmetry. These geometrical parameters are similar to those observed for Form I, the monoclinic polymorph (Marin *et al.*, 2013).

A search of the Cambridge Structural Database [CSD, V5.43, last update November 2022; Groom *et al.*, (2016)] for *N*-benzylideneanilines with no *ortho*-substituents on the aromatic rings, no errors, no polymerics, no ions or disorder, for organics only and $R < 0.05$ gave 220 hits. An analysis of the geometry of these 220 compounds (*Mercury*; Macrae *et al.*, 2020) indicated that the C═N bond length varies from 1.1775 to 2.202 Å, with a mean value of 1.269 Å (mean deviation of 0.009 Å). Hence, the value observed for Form II is significantly shorter at 1.243 (7) Å, while that for Form I is close to this average at 1.257 (2) Å. The bond lengths N1—$C1_{ar}$ and C7—$C1_{ar}$ have mean values of 1.420 (mean deviation of 0.006 Å) and 1.462 Å (mean deviation of 0.008 Å), respectively. The values observed for Form I are the same at 1.439 (3) Å, and for Form II they are also the same at 1.45 (2) Å, owing to the fact that both polymorphs are disordered about an inversion centre.

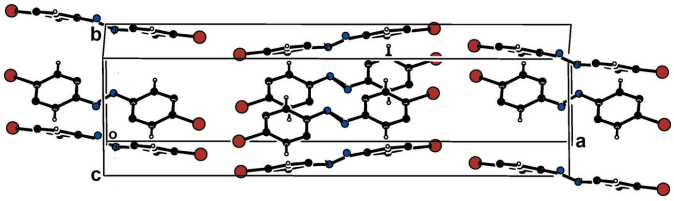

Figure 2
A view along the *c*-axis of the crystal packing of Form II of the title compound.

Table 1
Hydrogen-bond geometry (Å, °).

*Cg*1 is the centroid of the C1–C6 ring.

D—H···A	D—H	H···A	D···A	D—H···A
C2—H2···$Cg1^{i}$	0.95	2.81	3.535 (3)	134
C5—H5···$Cg1^{ii}$	0.95	2.78	3.494 (3)	133

Symmetry codes: (i) $x, -y-\frac{1}{2}, z-\frac{1}{2}$; (ii) $x, -y+\frac{1}{2}, z+\frac{1}{2}$.

Table 2
The relative contributions of the various interatomic contacts (Å) in the crystal structures of Form I[a] and Form II.

Contact	Form I[a]	Form II
	%	%
H···H	30.8	21.2
C···H/H···C	15.3	36.4
N···H/H···N	3.7	5.4
Br···H/H···Br	33.0	24.9
C···C	9.4	0.1
Br···C/C···Br	2.6	2.3
Br···Br	4.1	9.7

Note: (*a*) Marin *et al.* (2013).

3. Supramolecular features

In the crystal, the molecules are linked by C—H···π interactions (Table 1), forming columns stacking along the *b*-axis direction, as shown in Fig. 2.

4. Hirshfeld surface analyses and two-dimensional fingerprint plots for Form I and Form II

The Hirshfeld surface analysis (Spackman & Jayatilaka, 2009) was performed and the associated two-dimensional fingerprint plots (McKinnon *et al.*, 2007) were generated with *CrystalExplorer17* (Spackman *et al.*, 2021) following the protocol of Tan *et al.* (2019). The Hirshfeld surface is colour-mapped with the normalized contact distance, d_{norm}, from red (distances shorter than the sum of the van der Waals radii) through white to blue (distances longer than the sum of the van der Waals radii).

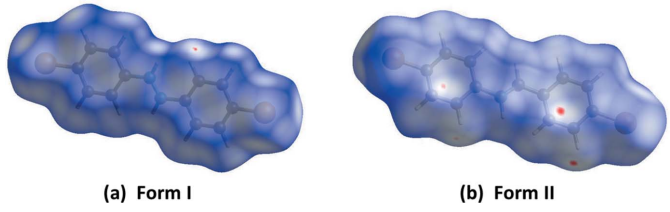

Figure 3
(*a*) The Hirshfeld surface of Form I, mapped over d_{norm} in the colour range −0.0139 to 0.7999 a.u. and (*b*) the Hirshfeld surface of Form II, mapped over d_{norm} in the colour range −0.0329 to 1.0662 a.u.

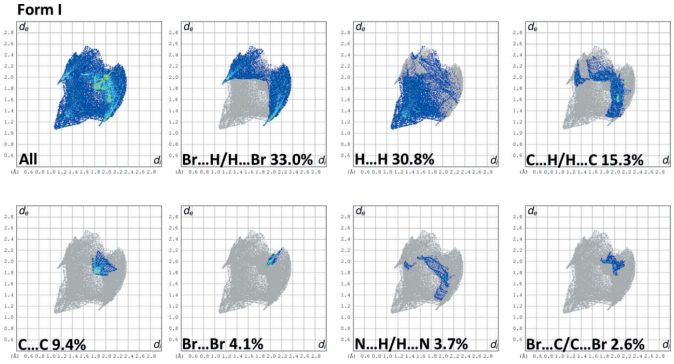

Figure 4
(*a*) The full two-dimensional fingerprint plot for Form I, and those delineated into Br···H/H···Br, H···H, C···H/H···C, C···C, Br···Br, N···H/H···N and Br···C/C···Br and contacts.

The Hirshfeld surfaces of Form I and Form II mapped over d_{norm}, are given in Fig. 3. The faint red spots indicate that short contacts are significant in the crystal packing of both compounds.

The full two-dimensional fingerprint plots for Form I and Form II are given in Figs. 4 and 5, respectively. There it can be seen that the relative contributions of the various interatomic contacts in the two polymorphs are significantly different (Table 2). For example, the C···H/H···C contacts have a major contribution (36.4%) in Form II whereas the same contact type is only 15.3% in Form I. This trend is reversed for the Br···H/H···Br contacts, which make a major contribution (33.0%) in Form I but less, 24.9%, in Form II, and for the H···H contacts which are greater in Form I (30.8%) compared to Form II (21.2%). The halogen···halogen interactions at the *para*-positions of the aromatic rings are more important in Form II (9.7%) compared to Form I (4.1%). Similar values of relative percentage are observed for the Br···C/C···Br contacts in Form I (2.6%) and Form II (2.3%). There are significant C···C intermolecular contacts observed for Form I (9.4%) but they are very weak (0.1%) in Form II. In contrast, the N···H/H···N contacts observed for Form II (5.4) are stronger than those observed for Form I (3.7%).

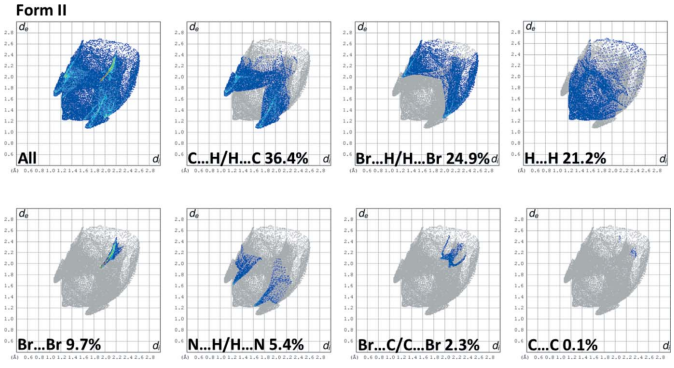

Figure 5
(*a*) The full two-dimensional fingerprint plot for Form II, and those delineated into C···H/H···C, Br···H/H···Br, H···H, Br···Br, N···H/H···N, Br···C/C···Br and C···C contacts.

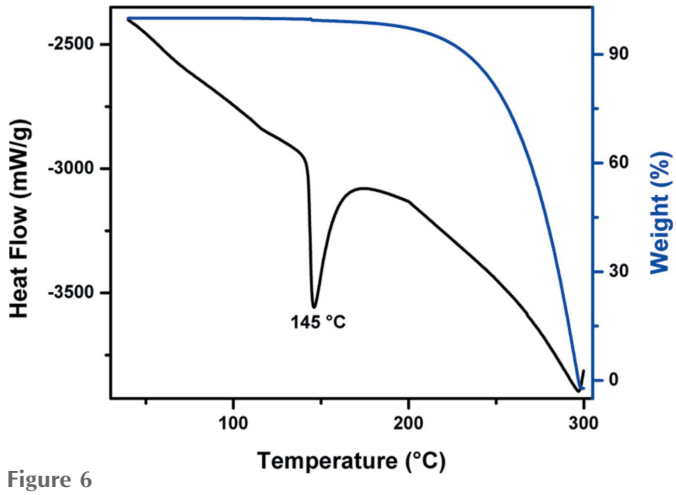

Figure 6
The TGA (blue) and DTA (black) curves for Form II.

5. Thermal properties

Thermogravimetric (TGA) and differential thermal (DTA) analyses were recorded using an S·T.A. – 1500 Simultaneous Thermo Analytical system in the temperature region 30–300°C at a heating rate of 10 K min^{-1} under a nitrogen atmosphere and alumina (Al_2O_3) was used as the reference material. The thermogravimetric and differential thermal analyses of Form II are shown in Fig. 6. In the DTA curve the sharp endothermic peak observed at *ca.* 145 °C corresponds to the melting point and indicates that there is no decomposition before melting. A single-stage weight loss is indicated in the TGA curve. At *ca* 300°C almost the entire mass of the sample is lost, thus indicating the occurrence of bulk decomposition.

6. Fluorescence spectra

The fluorescence emission spectrum of Form II at room temperature was recorded using a Horiba Jobin Yuon FLUOROLOG-FL3-11 spectrofluorometer in the wavelength range of 375–600 nm (Fig. 7). A powdered sample of Form II was excited at 375 nm and an emission peak was observed at

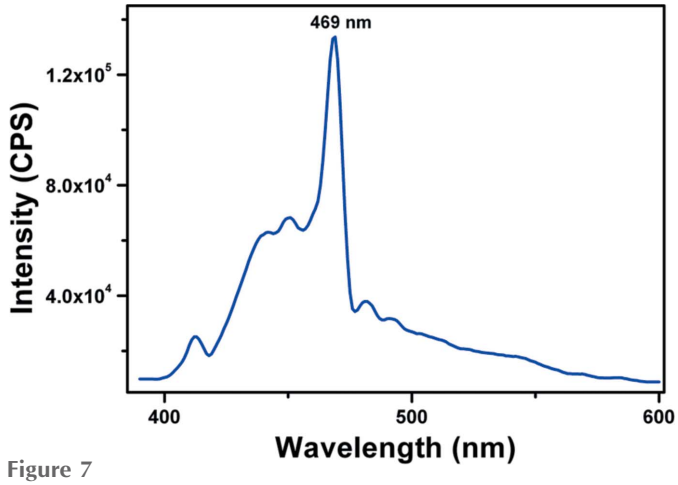

Figure 7
The solid-state fluorescence emission spectrum of Form II.

469 nm (blue colour) due to the presence of the aromatic rings (Lakowicz, 2006). For Form I, an emission peak was reported at 414 nm (weak violet colour) when excited at 278 nm (Marin *et al.*, 2013).

7. Z-scan studies

Employing the open aperture *Z*-scan technique the third order non-linear optical property of Form II was studied: the experimental setup has been described previously (Subashini *et al.*, 2013*a*,*b*). A sample of Form II was dissolved in chloroform, and 5 ns laser pulses at 532 nm were used for excitation. The optical density of the Form II solution is low at 532 nm, and its linear transmission is high (85%). The laser pulse energy reaching the sample was 100 µJ. The open-aperture transmission normalized to the linear transmission of the sample (normalized transmittance) was then plotted against the sample position measured relative to the beam focus and the non-linear absorption was indicated by a smooth valley-shaped curve, which was symmetric about the focal (Z = 0) position. The Z scan of pure chloroform was run separately to ensure that the solvent showed no non-linearity under the same experimental conditions.

The results of the open-aperture Z scan of Form II are shown in Fig. 8. An increase in absorption is found as the laser intensity is increased, thus indicating the non-linear optical absorption and the optical limiting behaviour of Form II. Since the linear transmission of the sample is ∼85%, the observed non-linear absorption might have contributions from genuine two-photon absorption (2PA), as well as from excited state absorption (ESA). For further details of the data analysis, see supporting information.

8. Synthesis, crystallization and spectroscopic analyses

The title compound was synthesized by the condensation reaction of 4-bromobenzaldehyde with 4-bromoaniline in an equimolar ratio: the reactants were dissolved in ethanol and refluxed for 6 h at 363 K, then cooled to room temperature. The precipitated product was purified by repeated recrystallization using ethanol as solvent. Colourless crystals of the title compound were grown at room temperature by slow evaporation of a solution in either ethanol or a mixture of methanol/chloroform (1:1).

The solid-state Fourier Transform Infrared (FT–IR) and Fourier Transform Raman (FT–Raman) spectra at room temperature (Fig. 9) were recorded using a Perkin Elmer grating infrared spectrophotometer (KBr pellet technique) and a Varian FT-Raman spectrometer, respectively, in the wave number range of 400–4000 cm^{-1} (Fig. 11). The C═N stretching vibration is observed as a strong band at 1630 cm^{-1} (IR) and at 1615 cm^{-1} (Raman) (Silverstein *et al.*, 2005). For Form I, the C═N stretching vibration was reported at 1620 cm^{-1} (Marin *et al.*, 2013). In the IR spectrum, the aromatic C═C stretching vibrations are observed at 1468 and 1562 cm^{-1}, and at 1474 and 1558 cm^{-1} in the Raman spectrum. In the IR spectrum, the aromatic C—H in-plane bending modes are observed at 1059, 1111, 1163 and 1230 cm^{-1} whereas the out-of-plane bending modes appear at 819 and 1000 cm^{-1} (Yoshino *et al.*, 2013). In the Raman spectrum, the corresponding in-plane bending modes are observed at 1008, 1067, 1098, 1165 and 1183 cm^{-1} whereas the out-of-plane bending mode is observed at 879 cm^{-1}. In the FT–IR spectrum, the band at 521 cm^{-1} is due to the aromatic C—Br stretching vibration.

The ^{1}H and ^{13}C NMR data for Form II in chloroform-D ($CDCl_3$) using tetramethylsilane as the internal standard were recorded employing a Bruker AC 400-NMR spectrometer.

The ^{1}H NMR spectrum (illustrated in Fig. S1 of the supporting information) exhibits five proton signals. The intense proton signal appearing at δ = 8.364 ppm is attributed to the imine group. The peaks at 7.48–7.52 and 7.59–7.61 ppm are due to the aromatic ring proton signals of the bromobenzaldehyde moiety and the peaks at 7.07–7.09 and 7.74–7.76 ppm are due to the aromatic ring proton signals of the bromoaniline moiety.

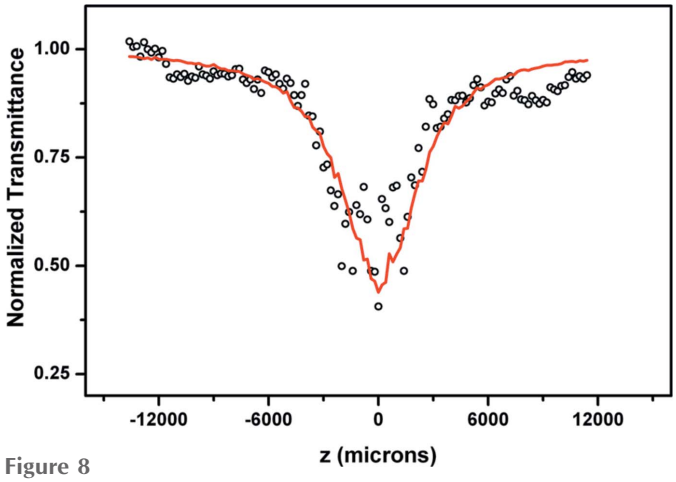

Figure 8
The open-aperture *Z* scan of Form II.

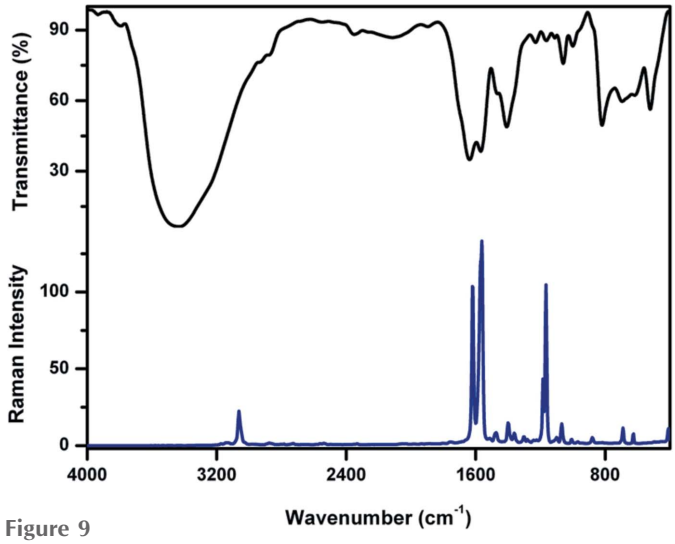

Figure 9
The FT–IR (black) and FT–Raman (blue) spectra of Form II.

Table 3
Experimental details.

Crystal data	
Chemical formula	$C_{13}H_9Br_2N$
M_r	339.03
Crystal system, space group	Orthorhombic, *Pccn*
Temperature (K)	173
a, *b*, *c* (Å)	27.4096 (19), 7.3301 (5), 5.9135 (3)
V (Å^3)	1188.11 (13)
Z	4
Radiation type	Mo *Kα*
μ (mm^{-1})	6.79
Crystal size (mm)	0.45 × 0.33 × 0.13
Data collection	
Diffractometer	STOE *IPDS* 2
Absorption correction	Multi-scan (*MULABS*; Spek, 2020)
T_{min}, T_{max}	0.411, 1.000
No. of measured, independent and observed [$I > 2\sigma(I)$] reflections	11334, 1125, 911
R_{int}	0.075
(sin $\theta/\lambda)_{max}$ (Å^{-1})	0.609
Refinement	
$R[F^2 > 2\sigma(F^2)]$, $wR(F^2)$, *S*	0.037, 0.061, 1.09
No. of reflections	1125
No. of parameters	71
H-atom treatment	H-atom parameters constrained
$\Delta\rho_{max}$, $\Delta\rho_{min}$ (e Å^{-3})	0.34, −0.48

Computer programs: *X-AREA* and *X-RED32* (Stoe & Cie, 2009), *SHELXS97* (Sheldrick, 2008), *SHELXL2018*/3(Sheldrick, 2015), *PLATON* (Spek, 2020), *Mercury* (Macrae *et al.*, 2020) and *publCIF* (Westrip, 2010).

In the ^{13}C NMR spectrum (illustrated in Fig. S2 of the supporting information) the peak at 76.46–77.40 ppm corresponds to the carbon atom of $CDCl_3$. A peak corresponding to the imine carbon atom is observed at δ = 159.26 ppm. The peaks at 119.60, 122.54, 134.88 and 150.54 ppm correspond to the phenyl carbon-atom signals of the bromoaniline moiety and the peaks at 126.19, 126.24, 130.19, 130.24, 132.09, 132.13, 132.24 and 132.29 ppm are due to phenyl carbon-atom signals of the bromobenzaldehyde moiety.

9. Refinement details

Crystal data, data collection and structure refinement details are summarized in Table 3. The atoms N1, C7, and H7 were refined with occupancies of 0.5 each. The C-bound H atoms were included in calculated positions (C—H = 0.95 Å) and refined as riding atoms with U_{iso}(H) = 1.2U_{eq}(C).

Acknowledgements

The authors thank the Central Instrumentation Facility, Pondicherry University, and the Advanced Instrumentation Research Facility, Jawaharlal Nehru University, New Delhi, for access to their analytical facilities. HSE is grateful to the University of Neuchâtel for their support over the years.

Funding information

AS thanks the University Grants Commission, New Delhi, for the award of a UGC Meritorious Fellowship [File No. 4-1/2008 (BRS)].

References

Bar, I. & Bernstein, J. (1977). *Acta Cryst.* B**33**, 1738–1744.
Bar, I. & Bernstein, J. (1982). *Acta Cryst.* B**38**, 121–125.
Bar, I. & Bernstein, J. (1983). *Acta Cryst.* B**39**, 266–272.
Bernstein, J. & Hagler, A. T. (1979). *Mol. Cryst. Liq. Cryst.* **50**, 223–233.
Bernstein, J. & Izak, I. (1975). *J. Cryst. Mol. Struct.* **5**, 257–266.
Bernstein, J. & Izak, I. (1976). *J. Chem. Soc. Perkin Trans. 2*, pp. 429–434.
Bernstein, J. & Schmidt, G. M. J. (1972). *J. Chem. Soc. Perkin Trans. 2*, pp. 951–955.
Caira, M. R. (2017). *Chemistry, Molecular Sciences and Chemical Engineering. Comprehensive Supramolecular Chemistry II*, pp. 127–160. Amsterdam: Elsevier.
Groom, C. R., Bruno, I. J., Lightfoot, M. P. & Ward, S. C. (2016). *Acta Cryst.* B**72**, 171–179.
Lakowicz, J. R. (2006). *Principles of Fluorescence Spectroscopy*, 3rd ed. New York: Springer.
Leela, S., Subashini, A., Reji, P., Ramamurthi, K. & Stoeckli-Evans, H. (2020). *Acta Cryst.* E**76**, 417–422.
Macrae, C. F., Sovago, I., Cottrell, S. J., Galek, P. T. A., McCabe, P., Pidcock, E., Platings, M., Shields, G. P., Stevens, J. S., Towler, M. & Wood, P. A. (2020). *J. Appl. Cryst.* **53**, 226–235.
Marin, L., Harabagiu, V., van der Lee, A., Arvinte, A. & Barboiu, M. (2013). *J. Mol. Struct.* **1049**, 377–385.
McKinnon, J. J., Jayatilaka, D. & Spackman, M. A. (2007). *Chem. Commun.* pp. 3814–3816.
Rolf, H. (2006). *Polymorphism in the Pharmaceutical Industry*. Wiley: Weinheim, Germany.
Sheldrick, G. M. (2008). *Acta Cryst.* A**64**, 112–122.
Sheldrick, G. M. (2015). *Acta Cryst.* C**71**, 3–8.
Silverstein, M., Webster, X. & Kiemle, J. (2005). *Spectrometric Identification of Organic Compounds.* Wiley, New York.
Spackman, M. A. & Jayatilaka, D. (2009). *CrystEngComm*, **11**, 19–32.
Spackman, P. R., Turner, M. J., McKinnon, J. J., Wolff, S. K., Grimwood, D. J., Jayatilaka, D. & Spackman, M. A. (2021). *J. Appl. Cryst.* **54**, 1006–1011.
Spek, A. L. (2020). *Acta Cryst.* E**76**, 1–11.
Stoe & Cie (2009). *X-AREA* and *X-RED32*. Stoe & Cie GmbH, Darmstadt, Germany.
Subashini, A., Bhagavannarayana, G. & Ramamurthi, K. (2013*a*). *Spectrochim. Acta A Mol. Biomol. Spectrosc.* **104**, 403–408.
Subashini, A., Leela, S., Ramamurthi, K., Arakcheeva, A., Stoeckli-Evans, H., Petříček, V., Chapuis, G., Pattison, P. & Reji, P. (2013*b*). *CrystEngComm*, **15**, 2474–2481.
Tan, S. L., Jotani, M. M. & Tiekink, E. R. T. (2019). *Acta Cryst.* E**75**, 308–318.
Westrip, S. P. (2010). *J. Appl. Cryst.* **43**, 920–925.
Yoshino, J., Kano, N. & Kawashima, T. (2013). *Dalton Trans.* **42**, 15826–15834.

supporting information

Acta Cryst. (2023). E**79**, 146-150 [https://doi.org/10.1107/S2056989023001111]

Synthesis, crystal structure and Hirshfeld surface analysis of the orthorhombic polymorph of 4-bromo-*N*-(4-bromobenzylidene)aniline

A. Subashini, K. Ramamurthi, R. Ramesh Babu, Reji Philip and Helen Stoeckli-Evans

Computing details

Data collection: *X-AREA* (Stoe & Cie, 2009); cell refinement: *X-AREA* (Stoe & Cie, 2009); data reduction: *X-RED32* (Stoe & Cie, 2009); program(s) used to solve structure: *SHELXS97* (Sheldrick, 2008); program(s) used to refine structure: *SHELXL2018*/3(Sheldrick, 2015); molecular graphics: *PLATON* (Spek, 2020) and *Mercury* (Macrae *et al.*, 2020); software used to prepare material for publication: *SHELXL2018*/3 (Sheldrick, 2015), *PLATON* (Spek, 2020) and *publCIF* (Westrip, 2010).

(*E*)-*N*,1-Bis(4-bromophenyl)methanimine

Crystal data

$C_{13}H_9Br_2N$
M_r = 339.03
Orthorhombic, *Pccn*
a = 27.4096 (19) Å
b = 7.3301 (5) Å
c = 5.9135 (3) Å
V = 1188.11 (13) Å^3
Z = 4
F(000) = 656
D_x = 1.895 Mg m^{-3}
Mo *Kα* radiation, *λ* = 0.71073 Å
Cell parameters from 8006 reflections
θ = 1.5–26.1°
μ = 6.79 mm^{-1}
T = 173 K
Plate, colourless
0.45 × 0.33 × 0.13 mm

Data collection

STOE IPDS 2 diffractometer
Radiation source: fine-focus sealed tube
Plane graphite monochromator
φ + *ω* scans
Absorption correction: multi-scan (MULABS; Spek, 2020)
T_{min} = 0.411, T_{max} = 1.000
11334 measured reflections
1125 independent reflections
911 reflections with $I > 2\sigma(I)$
R_{int} = 0.075
θ_{max} = 25.7°, θ_{min} = 1.5°
h = −33→33
k = −8→8
l = −6→7

Refinement

Refinement on F^2
Least-squares matrix: full
$R[F^2 > 2\sigma(F^2)]$ = 0.037
$wR(F^2)$ = 0.061
S = 1.09
1125 reflections
71 parameters
0 restraints
Primary atom site location: structure-invariant direct methods
Secondary atom site location: difference Fourier map
Hydrogen site location: inferred from neighbouring sites
H-atom parameters constrained
$w = 1/[\sigma^2(F_o^2) + (0.0216P)^2 + 1.2266P]$ where $P = (F_o^2 + 2F_c^2)/3$

$(\Delta/\sigma)_{max} < 0.001$
$\Delta\rho_{max} = 0.34$ e Å^{-3}
$\Delta\rho_{min} = -0.48$ e Å^{-3}

Extinction correction: (SHELXL-2018/3; Sheldrick, 2015), $Fc^{*}=kFc[1+0.001xFc^{2}\lambda^{3}/\sin(2\theta)]^{-1/4}$
Extinction coefficient: 0.0018 (2)

Special details

Geometry. All esds (except the esd in the dihedral angle between two l.s. planes) are estimated using the full covariance matrix. The cell esds are taken into account individually in the estimation of esds in distances, angles and torsion angles; correlations between esds in cell parameters are only used when they are defined by crystal symmetry. An approximate (isotropic) treatment of cell esds is used for estimating esds involving l.s. planes.

Fractional atomic coordinates and isotropic or equivalent isotropic displacement parameters (Å^2)

	x	*y*	*z*	U_{iso}*/U_{eq}	Occ. (<1)
Br1	0.20539 (2)	0.04724 (6)	0.54116 (7)	0.03603 (15)	
C1	0.06221 (13)	−0.0182 (5)	0.1208 (6)	0.0249 (7)	
C2	0.10666 (12)	−0.0797 (4)	0.0348 (6)	0.0263 (8)	
H2	0.107547	−0.136872	−0.109346	0.032*	
C3	0.14960 (12)	−0.0586 (5)	0.1562 (6)	0.0269 (8)	
H3	0.179825	−0.098688	0.095236	0.032*	
C4	0.14765 (12)	0.0211 (5)	0.3664 (6)	0.0234 (7)	
C5	0.10402 (12)	0.0822 (4)	0.4573 (6)	0.0241 (7)	
H5	0.103375	0.137253	0.602660	0.029*	
C6	0.06141 (12)	0.0622 (5)	0.3344 (6)	0.0247 (8)	
H6	0.031373	0.103567	0.396099	0.030*	
N1	0.0189 (6)	−0.0524 (16)	−0.013 (3)	0.0249 (7)	0.5
C7	0.0200 (8)	−0.0280 (19)	−0.026 (4)	0.0249 (7)	0.5
H7	0.023969	−0.080904	−0.171946	0.037*	0.5

Atomic displacement parameters (Å^2)

	U^{11}	U^{22}	U^{33}	U^{12}	U^{13}	U^{23}
Br1	0.02284 (19)	0.0454 (2)	0.0398 (2)	−0.00407 (19)	−0.00786 (17)	−0.0014 (2)
C1	0.0279 (12)	0.0196 (18)	0.0272 (15)	−0.0043 (13)	−0.0033 (11)	0.0045 (13)
C2	0.0331 (18)	0.0231 (19)	0.0229 (17)	−0.0017 (14)	−0.0001 (15)	−0.0011 (16)
C3	0.0257 (16)	0.028 (2)	0.0267 (19)	0.0032 (17)	0.0051 (14)	−0.0001 (17)
C4	0.0196 (15)	0.0229 (18)	0.0276 (18)	−0.0043 (14)	−0.0001 (13)	0.0045 (15)
C5	0.0287 (17)	0.0206 (19)	0.0229 (16)	−0.0023 (13)	0.0026 (15)	0.0005 (15)
C6	0.0191 (15)	0.0226 (19)	0.032 (2)	−0.0011 (15)	0.0016 (14)	−0.0002 (17)
N1	0.0279 (12)	0.0196 (18)	0.0272 (15)	−0.0043 (13)	−0.0033 (11)	0.0045 (13)
C7	0.0279 (12)	0.0196 (18)	0.0272 (15)	−0.0043 (13)	−0.0033 (11)	0.0045 (13)

Geometric parameters (Å, º)

Br1—C4	1.900 (3)	C3—H3	0.9500
C1—C6	1.394 (5)	C4—C5	1.385 (5)
C1—C2	1.395 (5)	C5—C6	1.383 (5)
C1—N1	1.448 (17)	C5—H5	0.9500
C1—C7	1.45 (2)	C6—H6	0.9500

C2—C3	1.387 (5)	N1—N1^{i}	1.30 (3)
C2—H2	0.9500	C7—C7^{i}	1.21 (4)
C3—C4	1.374 (5)	C7—H7	0.9500
C6—C1—C2	118.7 (3)	C3—C4—Br1	120.1 (3)
C6—C1—N1	123.8 (8)	C5—C4—Br1	118.4 (3)
C2—C1—N1	117.4 (7)	C6—C5—C4	119.4 (3)
C6—C1—C7	123.6 (9)	C6—C5—H5	120.3
C2—C1—C7	117.5 (9)	C4—C5—H5	120.3
C3—C2—C1	121.1 (3)	C5—C6—C1	120.5 (3)
C3—C2—H2	119.5	C5—C6—H6	119.8
C1—C2—H2	119.5	C1—C6—H6	119.8
C4—C3—C2	118.8 (3)	N1^{i}—N1—C1	119.0 (18)
C4—C3—H3	120.6	C7^{i}—C7—C1	123 (3)
C2—C3—H3	120.6	C7^{i}—C7—H7	118.3
C3—C4—C5	121.5 (3)	C1—C7—H7	118.3
C6—C1—C2—C3	−1.3 (5)	C4—C5—C6—C1	−0.1 (5)
N1—C1—C2—C3	−177.6 (5)	C2—C1—C6—C5	0.7 (5)
C7—C1—C2—C3	173.6 (6)	N1—C1—C6—C5	176.7 (6)
C1—C2—C3—C4	1.3 (5)	C7—C1—C6—C5	−173.9 (6)
C2—C3—C4—C5	−0.7 (5)	C6—C1—N1—N1^{i}	28.0 (17)
C2—C3—C4—Br1	178.5 (3)	C2—C1—N1—N1^{i}	−155.9 (13)
C3—C4—C5—C6	0.1 (5)	C6—C1—C7—C7^{i}	−2 (2)
Br1—C4—C5—C6	−179.1 (3)	C2—C1—C7—C7^{i}	−177.0 (15)

Symmetry code: (i) −*x*, −*y*, −*z*.

Hydrogen-bond geometry (Å, º)

*Cg*1 is the centroid of the C1–C6 ring.

D—H···*A*	*D*—H	H···*A*	*D*···*A*	*D*—H···*A*
C2—H2···*Cg*1^{ii}	0.95	2.81	3.535 (3)	134
C5—H5···*Cg*1^{iii}	0.95	2.78	3.494 (3)	133

Symmetry codes: (ii) *x*, −*y*−1/2, *z*−1/2; (iii) *x*, −*y*+1/2, *z*+1/2.